JOURNAL OF MATERIALS SCIENCE 15 (1980) 103–113

The microstructure of sintered Si–Al–O–N ceramics

M. H. LEWIS, A. R. BHATTI
Department of Physics, University of Warwick, Coventry, UK
R. J. LUMBY, B. NORTH
Lucas Group Research Centre, Solihull, W. Midlands, UK

Fine-grained ceramics, based on the substituted β'-Si_3N_4 crystal structure, have been prepared with near theoretical densities by pressureless sintering of compacts containing a large Y_2O_3 additive concentration. The microstructure contains two phases, β' and an Y/Al rich "silicate" glassy matrix, in the "as-sintered" condition. The matrix may be crystallized on heat treatment to a Si-substituted yttrium–aluminium garnet phase. The phase compositions and transformation mechanisms have been analysed by X-ray microanalysis, electron diffraction and imaging of thin sections.

A preliminary survey of mechanical properties of these sintered ceramics shows that they are comparable with commercial hot-pressed silicon nitrides, particularly at high temperatures. The possibility of development of a range of ceramic "alloys", dependent on their chemical environment and temperature of application, is discussed.

1. Introduction

Previous research on hot-pressed Si_3N_4 and Si–Al–O–N ceramics [1–3] has demonstrated, via electron microscopy and Auger electron spectroscopy, the important role played by an additive such as MgO in forming a low viscosity silicate liquid to effect the solution/reprecipitation mechanism for densification and transformation. The advent of Si–Al–O–N ceramics has enabled the formation of single phase materials by a solution of the unavoidable oxide surface layer (on α-Si_3N_4 particles) within the Al- and O-substituted (β') Si_3N_4 crystals. However, in carefully "balanced" Si–Al–O–Ns (which have elemental ratios given by the formula $Si_{6-z}Al_zO_zN_{8-z}$), to which 1% MgO has been added, there remains a residual Mg- and O-rich "segregate" layer which is detectable via Auger spectroscopy [3]. The composition of this segregate layer appears to influence the creep properties and susceptibility to subcritical crack growth in the same way as the composition of the clearly-visible silicate phase in commercial silicon nitrides [4]. These conclusions, together with the requirement for easier fabrication of fully-dense components of complex shape has indicated a need to study materials prepared with larger additive levels by sintering in the absence of applied pressure. The philosophy underlying these materials is the acceptance of a larger silicate liquid volume to enhance densification whilst attempting to control the composition and hence the mechanical properties of a residual phase which will be present in comparatively large volume fraction. One line of approach is to choose an additive composition such that the second-phase liquid solidifies as a stoichiometric crystalline phase just below the sintering temperature. If the crystal phase has an isotropic structure (avoiding weakly bonded cleavage planes typical of many silicates) and exhibits low dislocation mobility near to its melting point, relatively rapid viscous flow mechanisms of the glassy phases found in silicon nitrides will be avoided. The use of Si–Al–O–N based compositions is important in enabling a greater flexibility in choice of second phase composition than for materials with only Si, N and O contaminants. Also, the variable substitution level of the β'-phase should enable the accommodation of

0022–2461/80/010103–11$03.10/0

excess Si or Al which may result from crystallization of a stoichiometric second phase from a non-stoichiometric melt provided that the approximate O/N balance is achieved.

A previous paper [5] contained the results of some microstructural work on MgO-containing sintered Si–Al–O–N ceramics. The most prominent second phase, which crystallized on cooling from the sintering temperature, was a Si-substituted spinel ($Mg–Al_2O_4$). This occurs for a range of compositions since the spinel liquidus surface occupies a large area of the $MgO–Al_2O_3–SiO_2$ phase diagram. This relative inflexibility in choice of second phase, together with the refractory nature of hot-pressed silicon nitrides prepared with Y_2O_3 additions [6] indicates the need to study Si–Al–O–N ceramics sintered with variable quantities of a range of alternative additives. Sintered ceramics containing Y_2O_3 have been prepared with initial compositions corresponding to substitution levels $z \approx \frac{1}{2}$ and with varying O/N balance (see Table I). This paper describes a microstructural analysis of material in both the "as-sintered" and in the subsequently heat-treated conditions. A brief comparison is also made of the mechanical properties of the sintered and hot-pressed Si–Al–O–N ceramics.

2. Experimental techniques

2.1. Sintering

The powder charges for sintering were prepared by milling the weighed quantities of Si_3N_4, AlN, Al_2O_3 and Y_2O_3. The colloid milling, using isopropyl alcohol as a matrix, reduced all particles to $<5\,\mu m$ and ensured homogeneity of composition. The powders were dried and sieved before compacting. The material was preformed by cold isostatic pressing of 70 mm x 25 mm x 25 mm blocks in rubber envelopes at a pressure of $140\,MN\,m^{-2}$. Slip casting has also recently been used as an initial fabrication route. The preforms were enclosed in a bed of boron nitride within a graphite container which fitted into the susceptor of an inductively heated furnace. The sintering cycle consisted of a 1 h period to a maximum temperature of 1800° C at which isothermal sintering occurred for 1 h before "furnace" cooling by switching off the r.f. power. Specimens were examined either in this "as-sintered" condition or following heat treatments of up to 5 h at 1400° C. The surfaces of sintered specimens were cleaned before measurement of density by an Archimedian technique. Specimens were prepared from the sintered shapes by diamond cutting and grinding.

2.2. Electron microscopy and X-ray microanalysis

Electron transparent specimens were prepared from 0.2 mm thick diamond-cut slices by grinding to $<100\,\mu m$ on silicon carbide papers prior to ion-beam thinning using 5 keV argon ions at an incident angle of 40°. The specimen surfaces were evaporation-coated with a thin carbon film prior to examination in a JEOL 100C electron microscope equipped with an EDAX 707B energy-dispersive analysis system and a scanning-transmission (STEM) attachment.

3. Analysis of microstructure

3.1. Sintered densities

Exact analysis of residual porosity in two-phase sintered ceramics is difficult, because of an incomplete knowledge of the theoretical density of the second phase, especially in the glassy state, and the lack of precision in the experimental measurement of density by the Archimedian technique. The experimental densities listed in Table I may be compared with theoretical values based on a β'-Si_3N_4 with Al and O substitution of $z \sim 0.4$ together with the known density of "yttro-garnet" ($3Y_2O_3 \cdot 5Al_2O_3$) which is the crystalline form of second phase found in heat-treated materials (Section 3.2). Since the theoretical densities of β' and garnet phase are 3.16 and $4.55\,kg\,m^{-3}$ respectively, a ceramic with a volume fraction of ~5% second phase (estimated from the microstructure in thin sections) would have zero porosity if its measured density was $3.23\,kg\,m^{-3}$. The densities in Table I indicate porosity levels of ~2 to 3%. Scanning electron micrographs of polished or low-temperature fractured surfaces show pore sizes and densities which would give values of porosity <2%. Hence with careful control of powder processing and sintering cycle it is possible to achieve the "near-theoretical" densities associated with the hot-pressed Si–Al–O–N ceramics.

TABLE I

Ref. letter	Composition (wt %)				Density ($kg\,m^{-3} \times 10^3$)
	Si_3N_4	AlN	Al_2O_3	Y_2O_3	
A	92	4	4	6	3.125
B	92	5	3	6	3.152
C	92	6	2	6	3.175
D	92	7	1	6	3.147

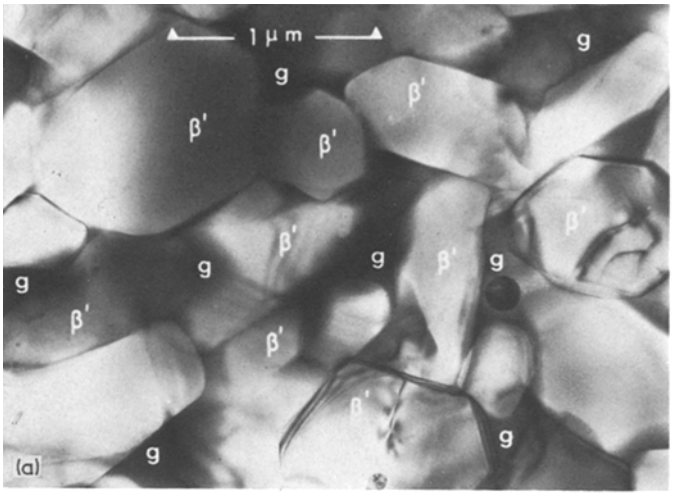

Figure 1 (a) Transmission electron micrograph of the "as-sintered" β'–glass matrix structure. The elongated prism morphology of β' crystals is shown in the scanning electron micrograph of a high-temperature fracture surface (b).

3.2. Transmission electron microscopy and diffraction

Ion-beam thinned sections from all compositions have similar microstructures consisting of ~0.5 μm β' crystals embedded in a matrix of second phase which is highly electron absorbing and hence is visible in dark contrast (Fig. 1a). There is ample evidence for the growth of β' into a liquid matrix, from their crystallographically faceted hexagonal prism morphology, characteristic of the solution/precipitation mechanism described previously for hot-pressed silicon nitride and Si–Al–O–N ceramics [1–3]. In this case the β' crystals have a larger ratio of their dimensions in hexagonal c and a directions; this is clearly visible in the 3D picture provided by high-temperature fracture surfaces recorded with a scanning electron microscope (Fig. 1b).

The electron-absorbing matrix is non-crystalline in as-sintered materials and crystalline in subsequently heat-treated materials. This can be ascertained in very thin sections from which clear selected area diffraction patterns may be obtained and which may be imaged with varying diffraction contrast. When the matrix phase in thin sections is highly diffracting (by tilting a selected area to rational orientation with respect to the electron beam) the contrast is high and uniform over large areas of thin section (Fig. 2a). This observation is similar to the sintered MgO additive materials, described in a paper [5], in which the spinel matrix phase has a constant orientation over ~10 μm^2, encompassing many β' grains. The constancy of matrix orientation in the Y_2O_3-containing sintered ceramics may be confirmed by selected area electron diffraction. Part of series of

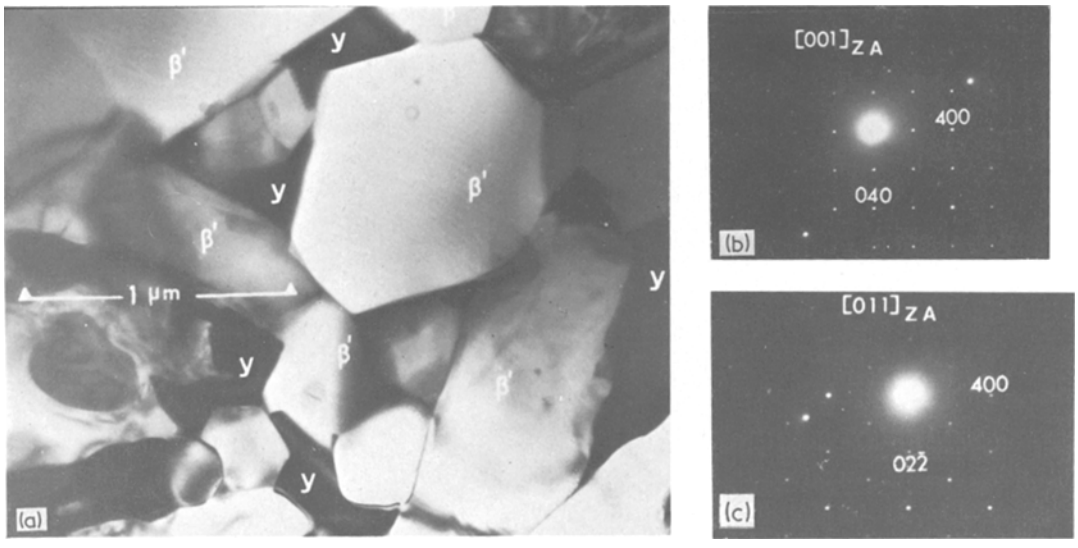

Figure 2 (a) Transmission electron micrograph of the β' garnet (Y) structure, in the heat-treated condition. The yttro-garnet phase is identified by electron diffraction patterns from the cubic crystalline matrix, (b) and (c).

such diffraction patterns taken with varying goniometer setting which are used in identifying the matrix lattice are reproduced in Figs. 2b and c. The lattice has cubic symmetry (lattice parameter 12.11 Å) and systematic absences in diffraction patterns which are consistent with the space group Ia3d. This information coupled with X-ray microanalysis (Section 3.3) identifies the phase as a Si-substituted form of "yttro-garnet" $3Y_2O_3 \cdot 5Al_2O_3$ (lattice parameter 12.01 Å [7]). This phase occurs in $z \approx \frac{1}{2}$ materials in the heat-treated state, except for specimen D. This material has a higher N/O ratio and may have been subjected to an higher than normal sintering temperature. The phase volume fraction is smaller than in specimen B, for example, as it contains a high yttrium and aluminium concentration (similar to B), but the crystal lattice has tetragonal symmetry with approximate parameters $a = 10.5$, $b = 10.4$ Å. This phase is tentatively identified as a substituted form of $2Y_2O_3 \cdot Al_2O_3$ (Warshaw and Roy [8] have suggested a "distorted cubic" cell of parameter $a = 10.40$ Å for the binary compound).

3.3. X-ray microanalysis

The use of energy dispersive X-ray analysis in conjunction with the high-resolution transmission electron microscope (TEM) and scanning transmission (STEM) unit enables quantitative analysis of phases which are $<0.1\,\mu m^2$ in area. This may be achieved either using the smallest (0.1 μm) diameter probe in conventional TEM imaging mode or with smaller probe sizes ($<0.01\,\mu$m) in the STEM mode.

A detailed analysis of phase compositions has been made for one of the series of specimens (B) as a basis for understanding the densification and crystallization mechanisms.

It is convenient to determine integrated peak intensities during analysis with the EDAX 707B system, but sample spectra from the β' and matrix phases are shown in Fig. 3. The expanded spectra compares the peak intensities for AlKα, SiKα and YLα characteristic X-rays. YKα (at ~15 keV), which is not complicated by overlap, is used for the quantitative analysis. Using corrections for (i) bremsstrahlung, (ii) peak overlap and for (iii) window absorption and efficiency of X-ray emission ([9], see Appendix) the approximate relative concentrations of Y, Al and Si are presented in Table II.

The most significant feature of the analysis is the marked reduction in Si concentration and enhancement of Al concentration in the second phase, in the crystallized state. The comparatively small change in Si/Al ratio in the β' crystals is probably due to their large volume fraction. Thus it appears that the major effect of heat-treatment is a diffusion of Si into β' decreasing their substitution level, and a reverse diffusion of Al into the second phase. The solubility of Y in β' is negligible (the Kα line is not detected within β'

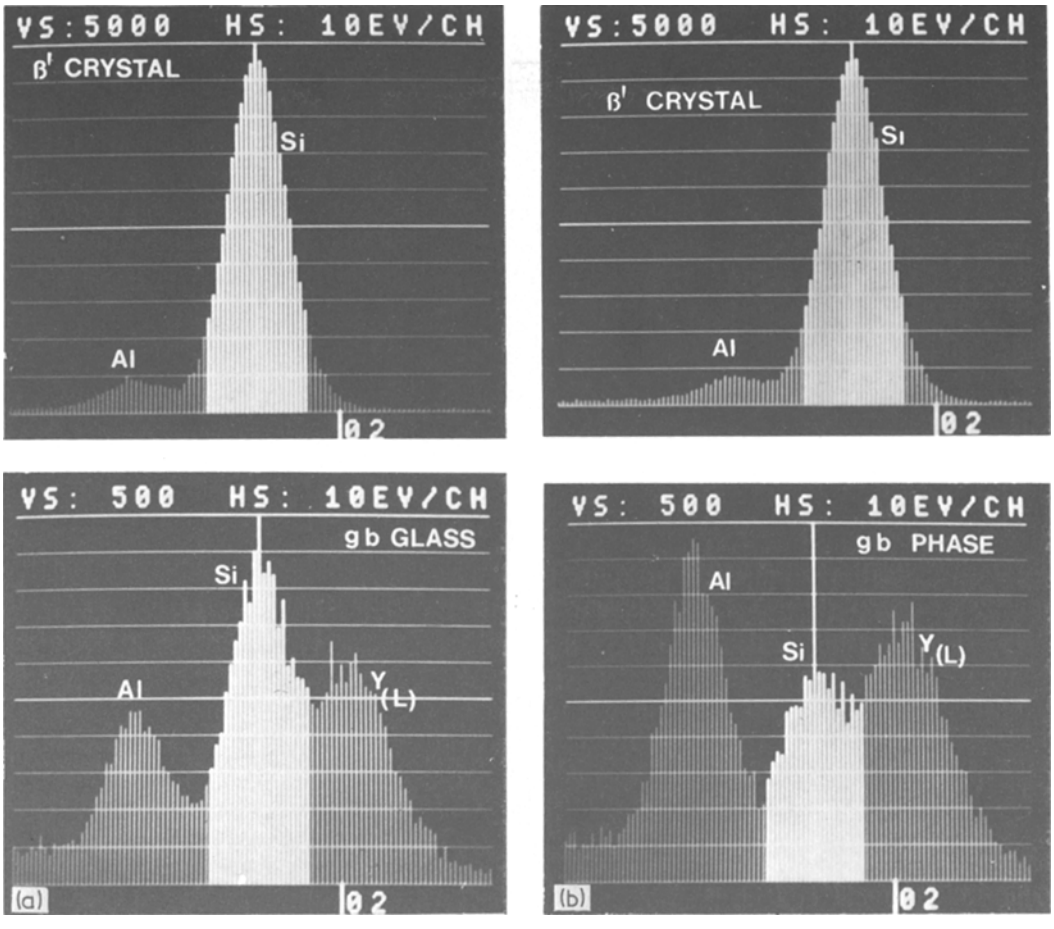

Figure 3 Energy-dispersive X-ray microanalysis of β and matrix phases in the (a) "as-sintered" and (b) heat-treated specimens.

even using a 0.3 μm probe) and hence may be used as a reference in determining elemental ratios. The approximate compositions of the second phases, neglecting the nitrogen content and assuming stoichiometric mixtures of Y_2O_3, SiO_2 and Al_2O_3 are

"sintered" $Y_2O_3 \cdot 2.36SiO_2 \cdot 0.68Al_2O_3$

"heat-treated" $Y_2O_3 \cdot 0.9SiO_2 \cdot 1.21Al_2O_3$

In the "thin-film" approximation [9] a simplification to the processing of measured intensities is provided by the ability to neglect absorption and fluorescence corrections. However there is evidence [10] that absorption becomes significant below the thickness limit for electron transparency in compounds for which the difference in the mass absorption coefficients, for the different emission lines, is large. The Appendix to this paper gives an example of this calculation and shows that for β' crystals preferential absorption of either SiKα or AlKα can be neglected for electron transparent sections. However, a calculation for YKα, YLα and AlKα from the "yttro-garnet" compound $3Y_2O_3 \cdot 5Al_2O_3$ shows that for a transparency thickness based on β' (which, being the major phase is frequently the criterion used in imaging) the correction factor for absorption may be large (a factor of 1.05 to 1.2 in the Al/Y ratio for typical thin sections). A factor of 1.05 is estimated to be appropriate in the above analysis for which the β' crystal thickness was measured (via the projected separation of contamination spots [11]) as

TABLE II

Sample B	Al	Y	Si
As sintered β'	1.0	0	12.67 ($z = 0.44$)
Glass phase	0.68	1.0	1.18
Heat-treated β'	1.0	0	14.0 ($z = 0.4$)
Crystalline 2nd phase	1.21	1.0	0.45

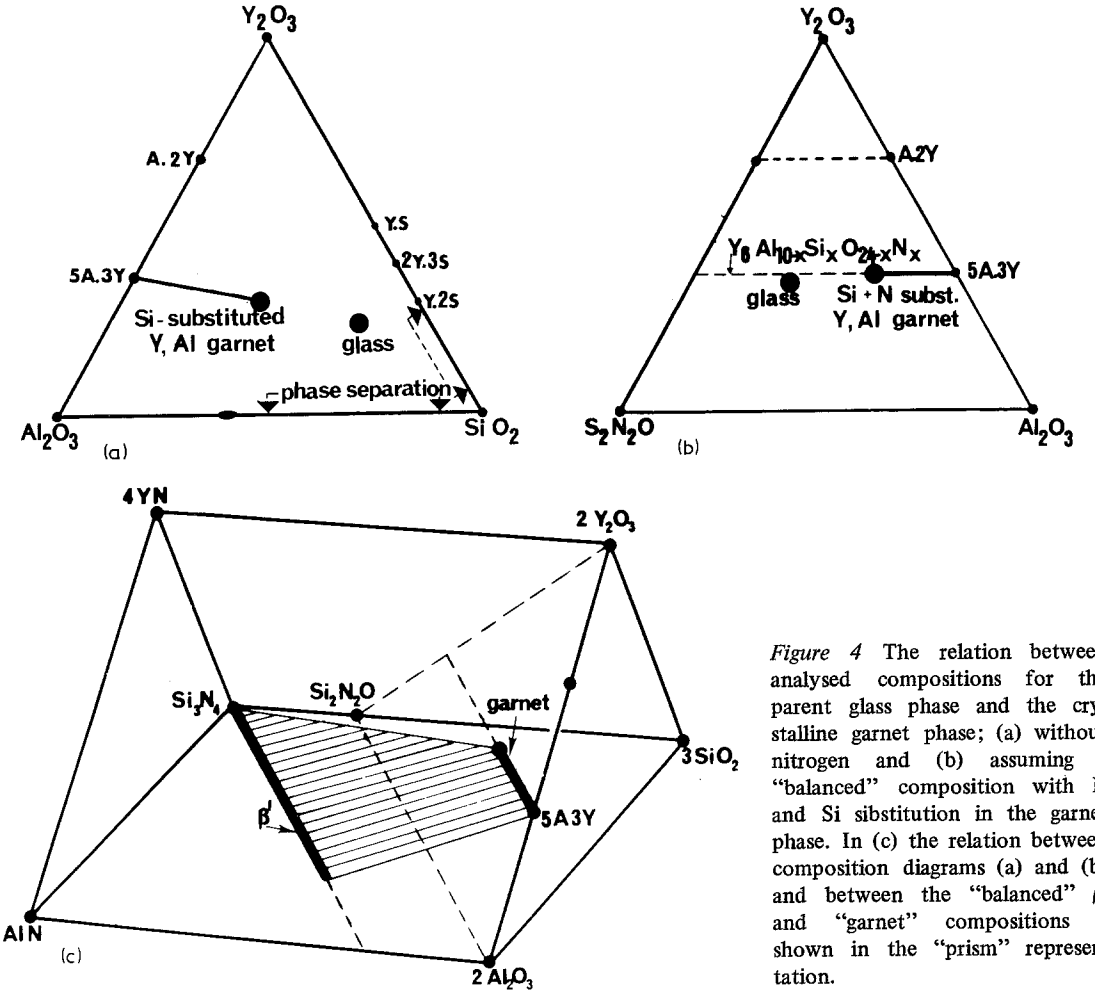

Figure 4 The relation between analysed compositions for the parent glass phase and the crystalline garnet phase; (a) without nitrogen and (b) assuming a "balanced" composition with N and Si sibstitution in the garnet phase. In (c) the relation between composition diagrams (a) and (b) and between the "balanced" β' and "garnet" compositions is shown in the "prism" representation.

0.15 μm. A similar absorption correction for the Si/Y ratio was calculated assuming a simple Si-for-Al substitution in the garnet crystal. Neglecting the small absorption correction the analysed composition for the Si-substituted garnet is consistent with this substitution model since the (Al + Si)/Y atomic ratio $\approx 5/3$. Fig. 4a shows the relation between the compositions of the parent glass phase, the substituted garnet and the $3Y_2O_3 \cdot 5Al_2O_3$ compound, assuming that oxygen levels are those appropriate to the stoichiometric components and that nitrogen is absent.

The absence of nitrogen would require that the substituted yttro-garnet contains either Y or Al vacancies (1 for every 3 substituted Si atoms). An unlikely alternative is oxygen interstitial formation. However, the most likely possibility is the simultaneous N-for-O substitution defining a general composition $Y_6Al_{10-x}Si_xO_{24-x}N_x$ for the garnet structure without vacancies. There have been previous reports of Si-substituted garnets in which "charge" compensation occurs via simultaneous substitution of Mn^{2+} for Y^{3+} [12] and Ca^{2+} for Y^{3+} [8]. The compositions of parent glass and substituted garnet crystal, assuming Si + N substitution, are shown in Fig. 4b. The relationship between the various stoichiometric terminal phases in Figs. 4a and b is indicated in Fig. 4c, which is drawn in the 3D prism representation used by Jack [13].

4. The sintering mechanism and phase transformation

Fig. 4 shows that the glass-phase composition in sintered materials is not far removed from the "disilicate" $Y_2O_3 \cdot 2SiO_2$. The liquidus in the Y_2O_3–SiO_2 system has a minimum (of $\sim 1600^\circ$ C) near to this composition and it is clear from this evidence and from the efficiency of the sintering process that it is the residue of a liquid silicate

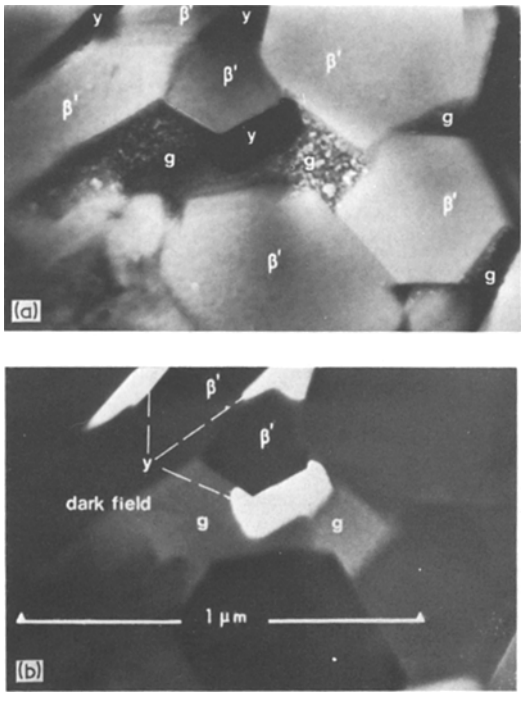

Figure 5 Partially crystallized microstructure showing the nucleation and growth of the garnet phase [identified by electron diffraction (a) and dark-field imaging (b)] at the β'–glass interface. The "mottled" contrast in the glass phase is produced by electron-irradiation damage during observation.

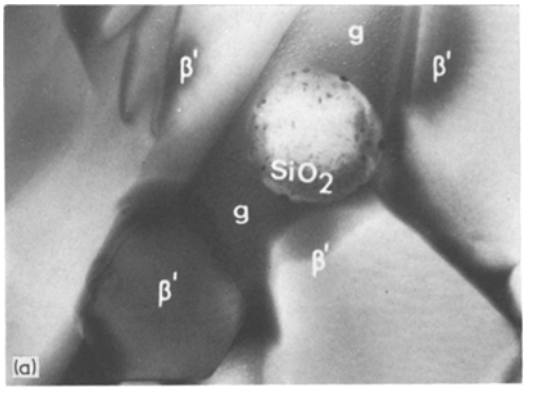

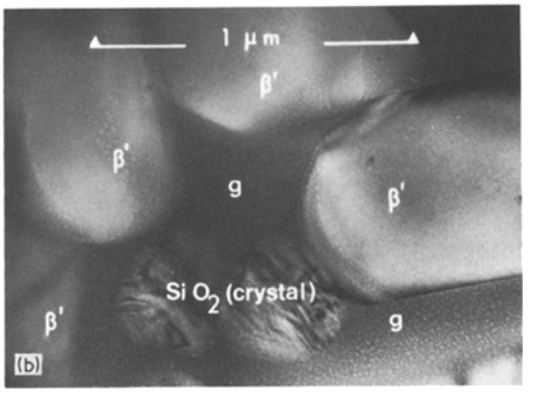

Figure 6 Occasionally observed globular SiO_2 glass-phase separation (a) and its subsequent crystallization (b) prior to garnet crystallization in the surrounding Y- and Al-rich glass.

phase at the sintering temperature (1800° C). The analysed composition is also consistent with its ability to form a glass on normal cooling. The sintering mechanism is that of; (i) yttrium-silicate liquid formation above ~1600° C, (ii) particle rearrangement, progressive solution of AlN, Al_2O_3 and, in part, of α-Si_3N_4, (iii) reprecipitation of the stable β form of Si_3N_4, with partial substitution of Al for Si and O for N. The process is similar to that for densification during hot-pressing but with a much larger liquid volume fraction to assist in the two main densification processes in the absence of applied pressure, namely particle rearrangement and solution-reprecipitation. The "driving force" for the latter is two-fold; (i) the difference in Gibbs free energy between α and β forms of Si_3N_4 (a transformation which is facilitated by relatively low activation energies for nucleation and growth within the liquid phase), and (ii) the reduction in surface energy per unit volume in transforming from the fine particle state (especially for the α-Si_3N_4) to the ~0.5 μm β' grain size.

Crystallization of the glassy matrix phase to form a substituted "yttro-garnet" is associated with the composition change analysed in the previous section. There are two possible explanations for this composition change; (i) the reduced temperature (from 1800 to 1400° C) may change the relative solubilities of Al, Si etc in β' and (liquid) matrix; alternatively the distribution in the "as-sintered" condition may be a non-equilibrium condition which results from a relatively slow solid state (β') diffusion process; (ii) crystallization of "yttro-garnet" occurs with the limiting Si substitution level (approximately $Y_6Al_7Si_3O_{21}N_3$) and the excess Si diffuses either into the β' crystals (together with nitrogen in exchange for Al and O) or into a glassy residue which occurs as a third phase between β' and the "yttro-garnet" crystalline phases.

Experimental observations on specimens which have been annealed for relatively short times (1 to

2 h) at 1400° C indicate that the composition change is the result of crystallization in the glassy phase. Fig. 5 is an example of partial crystallization of the yttro-garnet phase within a more Si-rich glassy matrix. (Quantitative analysis of the separate regions is not possible, because of phase overlap within the thin section.) Thus it appears that the exchange of Si and N for Al and O may occur either directly, by solid-state diffusion, at the β'/yttro-garnet crystal interface, or indirectly via the glassy parent phase. An important observation is that of a small quantity of residual glass as a third phase in well-annealed material. This is inhomogeneously distributed and its occurrence is influenced by the localized volumes of glass initially contained between β' crystal facets.

This analysis shows that the balance of initial chemical composition between Si_3N_4, AlN, Al_2O_3 and Y_2O_3 is important in determining not only the type of crystalline second phase in annealed microstructures but also in avoiding residual glassy phases which may be detrimental to high-temperature properties. This presence of this residual third phase will be influenced by the ability of β' and yttro-garnet phases to occur with variable composition. If the restriction to yttro-garnet composition is defined by the crystallographic principle of simple substitution (similar to β') then the optimum compositions for two-phase sintered products are likely to lie on the surface defined by the composition lines $Si_{6-z}Al_zO_zN_{8-z}$ and $Y_6Al_{10-x}Si_xO_{24-x}N_x$ (Fig. 4c). A precise definition of composition is not, however, always possible because of the unpredictable levels of surface oxygen in starting components. These restrictions do not apply when the second phase is retained in the glassy state.

An additional influence of composition is the ease of crystallization of the glassy phase. A "silicate" second phase rich in Y, Al or N is likely to have low viscosity and crystallize from the liquid state even on rapid cooling from the sintering temperature. The liquids formed in the series of compositions studied here, although effective in the sintering mechanism, must have comparatively high viscosities at temperatures below the equilibrium liquidus for the garnet phase. Hence they require prolonged heat-treatment for crystallization at 1350 to 1400° C. Even in the presence of a large β'–glass interfacial area, which should behave as a heterogeneous nucleation catalyst, few nuclei form within a large volume of material. The evidence for this is two-fold; (i) the constant crystallographic orientation of the garnet phase over very large electron transparent areas (typically 10 to 30 β' grain diameters), (ii) the presence of optically visible (1 to 2 mm) circular regions, of comparatively high reflectivity, sparsely distributed on polished surfaces in material which has been annealed for short times. Careful selection of electron transparent areas show these to be sections through spherical volumes of crystalline matrix which have grown from single nuclei. These single nuclei are believed to be internal microcavities but a precise correlation of the centres of highly reflective regions with cavities, observed on polished sections by scanning electron microscopy, is difficult because of their low density. The radii of the sphere of matrix crystallinity is similar to the depth of a layer observed at external surfaces. The preference for nucleation on free surfaces rather than β'–glass interfaces may result from a compositional influence in addition to the direct effect of surface energy, i.e. species may be lost to the vapour phase or may surface-segregate, reducing the local liquid viscosity or increasing the driving force for nucleation.

Secondary nucleation sites for crystallization are probably the regions of phase-separation, observed within the larger volumes of interfacet glass in sintered material (Fig. 6). This may be the result of heterogeneity in mixing which moves the liquid composition from the line a–b (in Fig. 4c) towards the SiO_2-rich corner, promoting liquid immiscibility (phase separation). The electron micrographs (Fig. 6b) indicate a crystallization of the SiO_2-rich globules prior to crystallization of the Y- and Al-enriched surrounding glass as yttro-garnet. This indirect nucleation process is in competition with the direct nucleation of the garnet phase on β'–glass interfaces or homogeneously in the glass phase. The dominance of a particular nucleation mechanism will depend mainly on the ratios of (Al + Y)/Si and O/N in the initial mixture.

5. Survey of mechanical and thermal properties

The mechanical and thermal properties of sintered Si–Al–O–N ceramics with Y_2O_3 additions, similar to the compositions described in this paper, have previously been surveyed by Lumby *et al.* [14]. In view of the comparatively large second-phase volume in these materials the high temperature mechanical properties are impressive. Creep resist-

ance is superior to that of a commercial (HS130) silicon nitride and approaches that of hot-pressed silicon carbide at a temperature and stress which are quoted requirements for ceramic turbine blades [15]. The fracture toughness (K_{Ic}) varies between 5 and 6 MPa $m^{1/2}$, the lowest values being obtained for heat-treated materials. These K_{Ic} values are comparable with the better hot-pressed "single-phase" Si–Al–O–N ceramics and silicon nitrides and the characteristic temperature – independence of K_{Ic} for Si_3N_4-based ceramics – is retained to higher temperatures. A rise in the apparent value of K_{Ic}, indicative of the onset of sub-critical crack growth, occurs between 1300 and 1350° C, the slightly higher "transition" temperatures occurring for the heat-treated materials.

The creep and K_{Ic} data confirm the dominance of composition rather than volume fraction of the second phase in controlling the high-temperature properties of ceramics based on β-Si_3N_4. The yttrium–aluminium silicate glass clearly has a high viscosity at 1300° C and its glass-transition temperature (based on the kinetics of its crystallization between 1300 and 1400° C) is probably $>1250°$ C. There is some evidence, from fracture surfaces of K_{Ic} specimens preserved in vacuum, that the mechanism for sub-critical crack growth is that of cavitation at β'–glass interfaces, initiated by viscous flow. The slightly higher "threshold" temperatures for sub-critical crack growth in heat-treated materials can then be explained by the absence of viscous flow in the crystalline garnet phase. Cavitation in these materials may be initiated by crystal plasticity or by β'–garnet interfacial sliding, similar to the β'–β' grain-boundary sliding observed in single-phase Si–Al–O–N ceramics [16]. Creep properties may be controlled by similar mechanisms, with crystal plasticity or viscous flow in the garnet phase being the rate-controlling process accommodating interfacial sliding in the absence of cavitation.

The small improvement in creep resistance and susceptibility to sub-critical crack growth for heat-treated materials is not reflected in modulus of rupture (MOR) values at the lower temperatures. There is also a variation in MOR with composition within both the "as-sintered" and heat-treated series studied here. For example, material B (Table I) is reduced from 794 to 750 MN m^{-2} on heat treatment. This suggests that the volume or modulus change accompanying inhomogeneous crystallization of the matrix glass may be responsible for the enhancement or initiation of a critical flaw. The variation in matrix viscosity, and hence in crystallization kinetics, with O/N ratio may also explain the MOR variation within the sintered series in which the initiation of inhomogeneously distributed spherical regions of crystallization has been detected. Materials C and D which should be progressively more susceptible to partial crystallization during normal cooling from the sintering temperature, have values of 564 and 520 MN m^{-2}, respectively. Recently prepared materials, with careful control of composition, homogeneity and heat-treatment, have improved and have made low-temperature properties more consistent.

Recent research on oxidation mechanisms in a range of hot-pressed and sintered Si–Al–O–N ceramics [17] has revealed an intrinsic limitation to the application of the two-phase (sintered) materials at the highest temperatures (1350 to 1450° C) in oxidizing environments. The outward diffusion of metallic ions from the second phase (yttrium in particular) into the initially protective glassy SiO_2 oxidation layer reduces its viscosity, increasing the rate of O and N transport and, ultimately, resulting in crystallization of the layer. A combination of the volume change on crystallization and the continued generation of N_2 gas bubbles at the oxidation interface causes the crystalline film to become porous and non-protective. Unlike the single-phase materials, in which metallic impurity ions (Mg, Ca) are progressively removed from the emergent grain boundaries (which act as diffusion channels), there is a constant supply of metallic ions from the surface of the matrix phase.

6. Ceramic "alloy" development

The limiting temperature imposed by oxidation of sintered materials coincides approximately with the limitation imposed by extensive subcritical crack growth. Hence one can forsee the need to optimize the thermal and mechanical properties of a range of ceramic alloys dependent on the temperature, stress and severity in oxidizing environment of intended application. From the lowest temperatures to ~1200° C the current attainment of properties which are comparable with the hot-pressed materials must favour the development of the more easily-fabricated sintered materials for application within this temperature interval. The refractory properties of the yttrium–aluminium silicate glass suggest little advantage in generating compositions specifically for ease of matrix crystal-

lization. However if ease of fabrication is necessary for load-bearing component application from 1200 to 1350° C then a choice of "balanced" composition on the "surface" between $Si_{6-z}Al_zO_zN_{8-z}$ and $Y_6Al_{10-x}Si_xO_{24-x}N_x$ is preferred. The improvement in susceptibility to sub-critical crack growth (or reduction in crack velocity for a particular stress intensity K_I) for the wholly crystalline ceramic will markedly increase the time to failure under creep conditions. For low-temperature applications the properties of materials prepared with large liquid content, for improved sinterability, should be explored. Such materials could be viewed as glass-geramic matrices containing variable volumes of β-Si_3N_4 crystal in dispersed form to enhance low temperature friction and wear properties and have potential application as bearing materials.

For the highest temperatures (1300 to 1450° C) the oxidation problem would dictate the use of single-phase hot-pressed materials. Use of the substituted β'-Si–Al–O–N has two particular advantages over commerically available β-Si_3N_4 products (such as HS130 or NC132); (i) the greater degree of control over the oxygen level by its substitution in β' crystals improves the key properties of creep resistance and resistance to subcritical crack growth*, (ii) the substituted Al^{3+} ions tend to counteract the viscosity-reducing tendency of impurity cations (Mg, Ca, Ma) within the silicate-glass protective oxidation layer. The latter property may also be the key to improved oxidation resistance of two-phase (sintered) materials, i.e. to ensure that the second-phase silicate is dominated by "intermediate" ions such as Al^{3+} to ensure the formation of high-viscosity, non-crystallizing protective silicate films. Since the compositions of the silicate protective film and of the liquid sintering aid are related, and the latter should possess high fluidity at the sintering temperature, this is an unlikely alternative to the single phase materials.

Appendix

Energy dispersive microanalysis in thin films

X-ray microanalysis of electron transparent thin films offers two important advantages over "bulk" analyses [in the scanning electron microscope (SEM)]:

(i) The ability to select areas $\ll 0.1\,\mu m$ in diameter for analysis, with very limited "spreading" of the analysed volume with depth below the electron beam entry surface, i.e. the analysed volume depends mainly on probe diameter and not, as in SEM, on the beam penetration. The transmission electron microscope used in this research programme is fitted with a scanning transmission attachment which enables probe diameters of $< 0.01\,\mu m$ to be used (however the minimum probe size usually depends on the X-ray count rate obtainable, which varies with atomic number and specimen thickness).

(ii) The mathematical models which relate X-ray intensities to element concentrations can be simplified by neglect of "absorption" and "fluorescence" corrections. The validity of this assumption is discussed below in terms of a simplified "absorption" correction with varying specimen thickness.

Hence a simple model relating intensity ratios (I) for two elements with their concentration (C) is given by:

$$\frac{C_1}{C_2} = K_{12}\frac{I_1}{I_2}$$

where K_{12} is the correction factor for ionization cross-section, fluorescent yield, and detector efficiency for X-rays from the two elements.

The values of K_{12} used in this analysis are taken from a paper by Russ [9] who has tabulated K-values for all elements for Kα, Lα and M X-ray lines. A similar treatment has been given by Goldstein *et al.* [10] and there is close agreement in calculated K-values for Kα lines of elements up to $z = 39$ (yttrium).

Absorption correction

A simplified absorption correction can be obtained [10] by assuming that the average depth for X-ray excitation occurs at $t/2$, where t = specimen thickness. Thus:

$$\frac{K\,(\text{thick})}{K\,(\text{thin})} = \frac{K'_{12}}{K_{12}} \approx$$

$$\exp -\left(\frac{\mu_2}{\rho} - \frac{\mu_1}{\rho}\right)(\sec\alpha\cot\alpha)(\rho t/2)$$

where μ_1/ρ = mass absorption for Kα line from element 1 in the compound of density ρ, and α =

*Careful control of the impurity additive type and oxygen levels has produced a material which undergoes an entirely diffusion-controlled creep deformation, without cavitation, in the temperature interval 1200 to 1450° C [16].

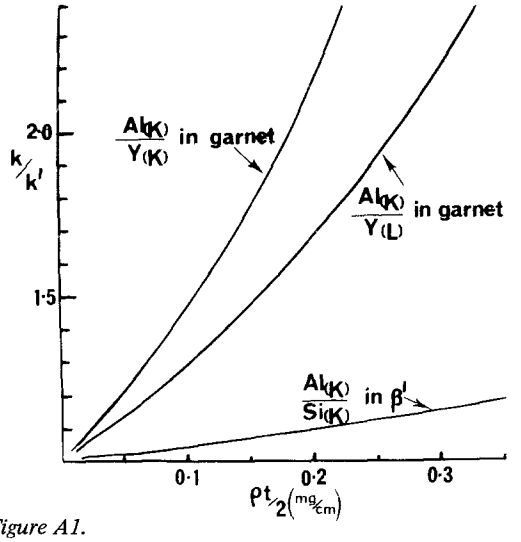

Figure A1.

X-ray take off angle for the particular geometry (in practice $\alpha \approx 45°$).

Values of μ/ρ are calculated from the tables due to Heinrich [18] using the expression:

$$\frac{\mu}{\rho} = \frac{n}{\rho V_c} \sum \frac{\mu}{\rho_i} \frac{A}{N}$$

where the summation is over all atoms in 1 molecule, n = number of molecules per unit cell, V_c = unit cell volume, A = atomic weight, and N = Avogadro's number.

Calculations of K'/K for the β' and yttro-garnet phases are summarized in Fig. A1. For normal electron transparent sections (β' thickness 0.05 to 0.06 μm) the correction is negligible for the Al/Si ratio in β' but could be as large as ~ 1.3 for the Al/Y ratio in the garnet phase.

References

1. P. DREW and M. H. LEWIS, *J. Mater. Sci.* 9 (1974) 261.
2. B. D. POWELL and P. DREW, *ibid.* 9 (1974) 1867.
3. M. H. LEWIS, B. D. POWELL, P. DREW, R. J. LUMBY, B. NORTH and A. J. TAYLOR, *ibid.* 12 (1977) 61.
4. M. H. LEWIS and G. SMITH, in "Advances in Research on the Strength and Fracture of Materials", edited by D. M. R. Taplin (Pergamon, Oxford, 1977).
5. M. H. LEWIS, A. R. BHATTI, R. J. LUMBY and B. NORTH, *J. Mater. Sci.* (in press).
6. G. E. GAZZA, *Bull. Amer. Ceram. Soc.* 54 (1975) 778.
7. M. L. KEITH and R. ROY, *Amer. Mineral.* 39 (1954) 1.
8. I. WARSHAW and R. ROY, *J. Amer. Ceram. Soc.* 42 (1959) 434.
9. J. C. RUSS, in "Microprobe Analysis Applied to Cells and Tissues", edited by T. Hall, P. Echlin and R. L. Kaufmann (Academic Press, New York, 1974) p. 269.
10. J. I. GOLDSTEIN, J. L. COSTLEY, G. W. LORRIMER and S. J. B. REED, in "SEM/1977," edited by O. Johari (IITRI, Chicago, 1977) paper 46.
11. G. W. LORMER, G. CLIFF and J. N. CLARK in "Developments in Electron Microscopy and Analysis", EMAG 75, edited by Venables (Academic Press, London, 1976) p. 153.
12. H. S. YODER and M. L. KEITH, *Amer. Mineral.* 36 (1951) 519.
13. K. H. JACK, *J. Mater. Sci.* 11 (1976) 1135.
14. R. J. LUMBY, B. NORTH and A. J. TAYLOR, Proceedings of the 5th AMMRC Materials Technology Conference, Newport, RI (1977).
15. R. N. KATZ and E. M. LENOE, Army Materials and Mechanics Research Centre, (AMMRC) SP 75-4 (1975).
16. B. S. B. KARUNARATNE and M. H. LEWIS, *J. Mater. Sci.* (in press).
17. M. H. LEWIS and P. BARNARD, *J. Mater. Sci.* (in press).
18. K. F. J. HEINRICH, in "A Manual of Quantitative Electron Probe Microanalysis" (Structure Publications Ltd., 1970).

Received 28 March and accepted 26 April 1979.